COMPUTATION AND SYNTHESIS OF METAL CATION COMPLEXES

A thesis submitted to
The Honors Program at UDM in partial fulfillment of the requirements
For graduation with honors

By

Alexis Konja

May 2014

Computation and Synthesis of Metal Cation Complexes

A Thesis written by

Alexis C. Konja

Approved by

Jonathan Stevens

Committee

Mark A. Benvenuto, Professor of Chemistry

Matthew J. Mio, Associate Professor of Chemistry

Salomeia S. Schlick, Professor of Chemistry

Accepted by

Jason J. Roche, Assistant Professor of Communication Studies

Approved By:

Primary Thesis Director

Committee:

Accepted by:

Director of the Honors Program

Table of Contents

Preface

When beginning my work with Dr. Stevens in the department of chemistry at the University of Detroit Mercy, I never imagined that the lab work I had conducted thus far becoming what my thesis would entail. I joined Dr. Steven's research after my freshman year as a biochemistry student, obtaining a fellowship to do summer research summers of 2011 and 2012. The next eight semesters would be filled with a mix of computational chemistry with a little bit of synthesis. My work started with the different metal complexes that would correlate with Dr. Mio's research and the study of the Sonogashira reaction. I would not learn about this reaction until my second semester of advanced synthesis lab. Then, I began to work on a model that resembled a ligand byproduct, 4, 4'-diaminodiphenylmethane that Dr. Benvenuto's lab was studying. This was not until the end of my sophomore year where I agreed with Dr. Stevens that this is what would become my thesis. Utilizing different components from the research teams at the University of Detroit Mercy, I have broadened my understanding of the applications of computational chemistry. It had been a difficult journey considering I was introduced to the concepts and mathematics of the computations until my senior year, in physical chemistry. However, immersing myself in the computational research at hand allowed me to gain an understanding of the application in real world practice. The confidence in my work was solidified not only from the constructive criticism and gratification received during poster sessions and American Chemical Society meetings. My assurance was congealed upon hearing Dr. Bill Carrol (past president of the American Chemical Society) sent his accolades into the crowd as he spoke at the university in April of 2013, describing how important it was that computational chemistry needed to be utilized throughout the world of research as a way to conserve materials and help create concrete hypotheses of syntheses. My work with Dr. Stevens has not only been a way to develop my thesis. It was an outlet of knowledge in order to create a strong skill set and background for chemical and biochemical research that I may conduct later in life. Overall, I have been able to present my work at various conferences held

by the American Chemical Society, presenting at local, regional, and national meetings in Detroit, Lansing, New Orleans, and Dallas, respectively. I have also had the pleasure of having the work fully recognized and awarded by the University of Detroit Mercy, College of Engineering and Science and Michigan State's Undergraduate Research Symposium.

Abstract

This thesis discusses two projects. The first project (project A) used Hartree-Fock and M052X hybrid density functional theory (DFT) calculations and several different basis sets to optimize transition metal-acetylene complexes. Successful calculations of structures that complex to transition metals with a (+1) or (+2) charges have been studied. The goal is analysis and improvement of a method of synthesis common in organic chemistry. A second project (project B) involving cation-ligand complexes employs calculations using Hartree Fock and B3LYP hybrid DFT methods as well as a 6-31G(d) basis set. In addition to the computations, laboratory synthesis of multi-dentate ligands which may chelate with various transition metals has begun. The goal of the research is the development of ligands useful for removal of metal contaminants from water sources. Future synthesis will attempt to chelate ligands with Fe^{3+}, Zn^{2+}, and lanthanides.

Introduction:

Project A: **Acidity of Transition metal-C_2H_2 Complexes Observed in an Attempt to Improve the Trans-Metalation of the Sonogashira Side-Reaction**

The presence of metal ions often catalyzes reactions. Sonogashira reactions are multistep coupling reactions that result in alkynes linking to aromatic organic halides.[1-4] While the reaction mechanism is not fully understood, it is believed to occur by means of formation of a copper-acetylene complex in which C_2H_2 associates with Cu^+ ions. [5,6]

A research group from the Department of Chemistry and Biochemistry at the University of Detroit Mercy has designed a Sonogashira reaction that can take place between 25-45 min., in contrast to the reaction currently studied which takes approximately 18 hours to run. An attempted Sonogashira reaction that did not incorporate the correct catalysts reported negative feedback. Once the correct catalysts were reincorporated, including copper iodide, the Sonogashira reaction was successful.[7] Another research group has made significant progress considering the researchers were able to devise and test a reaction that disregarded the use of a copper catalyst. At the College of Chemistry in Beijing, the research group has devised a reaction that can catalyze and complete a Sonogashira reaction without the presence of copper. The reaction that takes place can run at room temperature or at a lower temperature with the presence of other sparging solutions. The data shows that the yields of the multiple reactions tested were favorable.[8] Another biomedical reaction incorporates the Sonogashira coupling reaction that is catalyzed under microwave conditions.[9] This gives rise to energy and time conservation as the reaction does not need to sit overnight in order for complete synthesis to occur. From a more pharmaceutical perspective, the Sonogashira reaction has been explored in order to generate consecutive reactions. A medical group in Sweden is studying the effects of multiple Sonogashira reactions in order to synthesize a protein to aid the recovery of patients diagnosed with tuberculosis.[10] Continued research of the Sonogashira reaction will carry on considering all the possibilities the reaction holds. Currently, the complete reaction mechanism has not been described, allowing for a competitive amount of research on this particular reaction. The research currently being discussed goes on to explore the flexible efficiency of the Sonogashira reaction's side cycle involving a copper catalyst. The challenge at hand is attempting to utilize a different metal which is more efficient as well as cheaper than copper.

The Sonogashira reaction has a flexible reaction environment and is useful for forming single, double, and triple bonded carbons based on the reagents used in the reaction. Although the mechanism

of the entire reaction remains unknown, there are two parts of the reaction that are clear. The two types of catalysts used include a palladium catalyst and copper co-catalyst. The two different catalysts have their own cycle. The product of these side cycles is then incorporated into the reaction. As the reaction is taking place, it begins with a palladium catalyst which reacts with the carbon functional group present as the second reagent. These are generally alkenes or acetylenes.

A palladium intermediate is then formed after the reaction takes place between the carbon functional group and the palladium catalyst. Once this is formed, it is thought to be the rate limiting step of the reaction. Referring to **Figure 1**, an important step in the process is the formation and deprotonation of copper acetylide, complex F in the copper cycle. This creates complex C and the copper halide is expelled, creating complex G. Comparing the ligands, they are both trans and switch to cis formation as trans-cis isomerization occurs. This produces complex D viewed in the cycle pictured in **Figure 1**. Lastly, complex D undergoes reductive elimination producing the alkyne. From this step, the palladium catalyst may regenerate. As the copper cycle continues, complex E is formed because of the presence of base in the reaction flask. The terminal protons on the alkyne now are more acidic which leads to the formation of the copper acetylide or compound F in the picture shown below. Therefore, as complex F continues to react with complex B, the regeneration of complex G will remain steady so long as the cycle is not disrupted. [11] Generally, the second row transition metal that is used in the coupling step is copper with a (+1) oxidation state. Our research in the University of Detroit Mercy computational chemistry laboratory is testing the Sonogashira reaction coupling step to see if the ligand being tested will bind to other second and third row transition metals. The transition state of these metals is also a variable in that (+1) and (+2) metal complexes have so far been computed.[12]

As noted above, the reaction is thought to occur by means of formation of a copper-acetylene complex in which C_2H_2 associates with Cu^+ ions. This is followed by deprotonation of the acetylene. The

addition of the C_2H_2 molecule to the metal should make the metal more acidic, i.e., formation of the complex facilitates deprotonation.

Recent experimental research based on calculations I have modeled has shown that it is possible to use metal cations other than Cu^+ to catalyze Sonagashira reactions.[12] However; this research has not focused on which metals make the most effective co-catalyst. The best co-catalyst should be the metal that makes acetylene most acidic on complexation. This research is intended to model the deprotonation of the acetylene complex while bonded to metals of the first and second transition row. *Ab initio* density functional molecular orbital calculations were used in order to calculate the change in energy and enthalpy for acetylenes bonding with transition metals. The enthalpies of the complexes are also calculated; the lower this enthalpy, the more acidic the cation-acetylene complex. Results suggest other metals may be more efficacious than copper as a co-catalyst. Thus, in application with the Sonogashira reaction, other metals are currently being tested in order to predict other efficient side reaction possibilities.

These predictions were compared to the quantitative yields of synthetic attempts which implement these ions in the co-catalyst role. Correlation is observed between the theoretically-predicted acetylene complex energies and the utility of the transition metal co-catalysts as measured by percent yields (verified by GC-MS analysis) in a common Sonogashira transformation. This Sonogashira synthesis with varying co-catalysts is currently being attempted by the Mio research group at the University of Detroit Mercy. Complete experimental work-up and procedure is not yet available. The computations were completed by our research group and are summarized in the computational results.

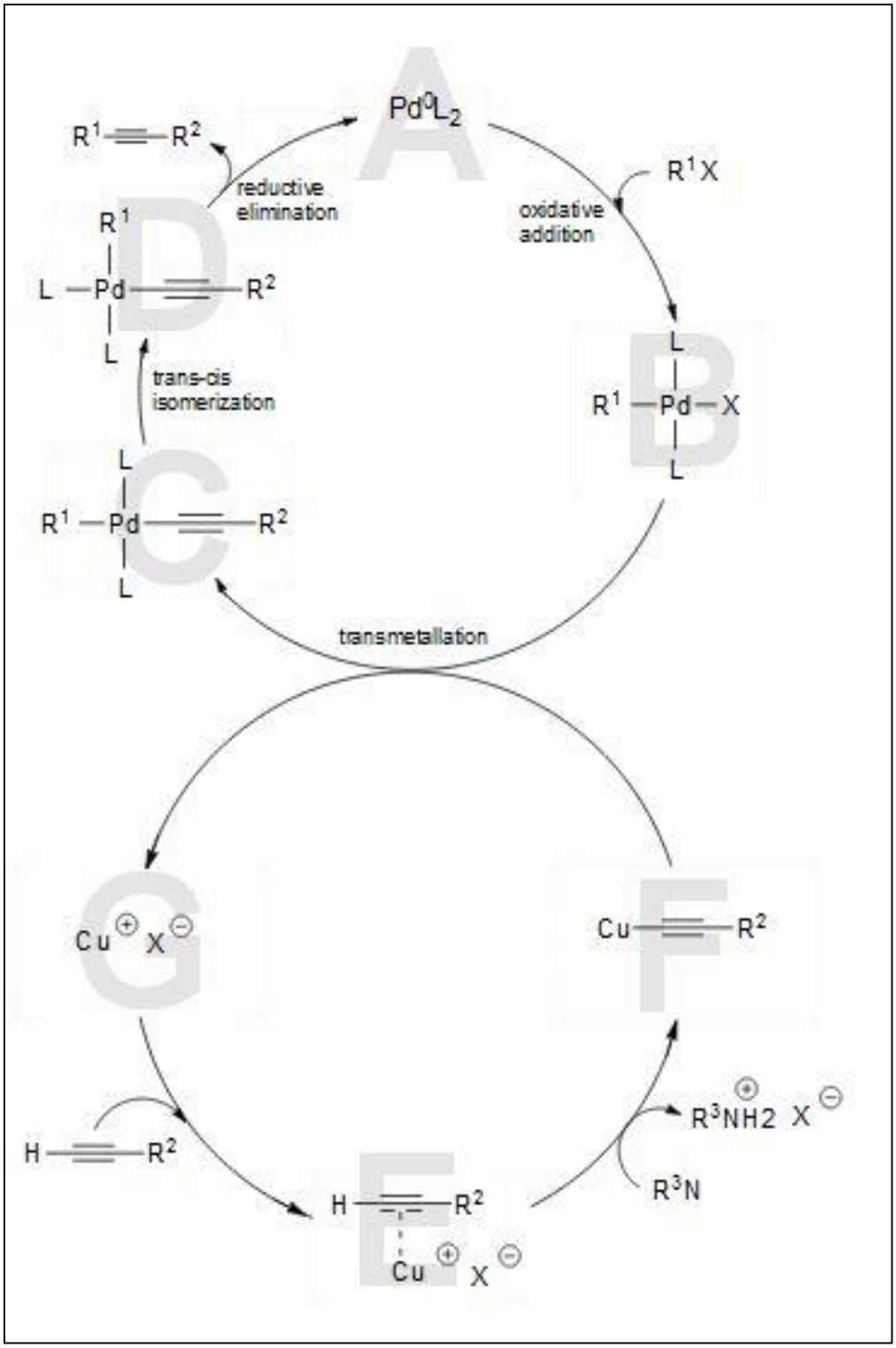

Figure 1: The palladium and copper catalyst cycles of the Sonogashira reaction. The primary focus of this research is cycle portions G-E-F.[13]

Project B: **Synthesis and Computation of complexes of Iron and Zinc with large molecular ligands**

Coordination chemistry is essentially the study of bound molecules or anions that are in turn known as ligands or complexing agents which can bind to create metal-containing compounds. The synthesis of ligands with the metals generates the compounds, in this study, in highly multi-dentate ligand-metal complexes. Potential uses of such materials could be in real world solutions for the remediation of polluted water, or in the distant future regarding molecular switches and computing devices.

There remains enormous potential in this field for the development of new materials from byproducts of reactions currently taking place in the industry. With these chelating agents, there is the possibility of generating metal removal applications in the environment. This research is part of a collaborative effort to make, characterize, and examine a series of multi-dentate ligands and the metal complexes. Computation may be able to help characterize the IR spectra of ligands and complexes formed by the Benvenuto synthesis group at the University of Detroit Mercy. Two ligand syntheses have been successfully attempted thus far, as seen in **Figure 2** below. Proton NMR has been used In order to verify that these ligand structures are properly synthesized.

Fourier transformed Infrared spectroscopy data has also been gathered for all these ligands, and will be compared to the vibrational frequencies of computational model structures. The structures of small “model ligands” and their complexes with Fe^{3+} and Zn^{2+} have been optimized using Hartree Fock and B3LYP DFT and a 6-31G(d) basis set. The structures of these model compounds were calculated in order to observe the geometry, feasibility, and stability of these ligands and their complexes as well as provide the predicted IR spectra for eventual comparison with the synthetic data. One idea is to compare relative binding energies between the ligands and different metals. This is done in order to observe the feasibility of chelation with regards to different ligands and with regards to different metals.

Lastly, the aim is to utilize the byproduct in synthesis with the above mentioned metals in order to possibly observe chelation.

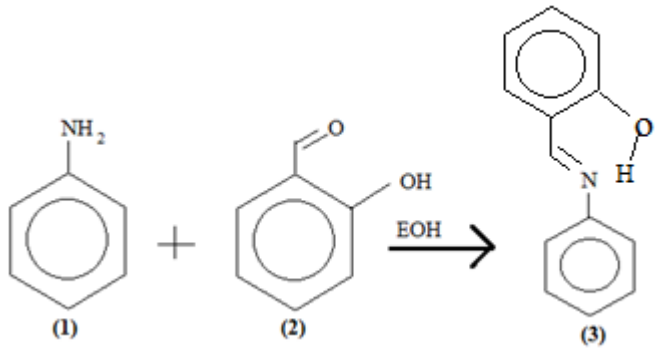

(α)

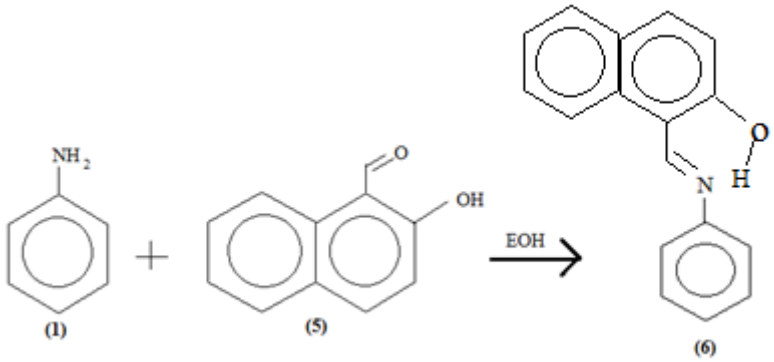

(β)

Figure 2: (α): The first synthetic reaction studied; a part of what the Benvenuto group likes to classify as the simple six ligand reactions. **(1)** aniline, **(2)** salicylaldehyde, **(3)** salicylideneaniline. **(β)** The second synthetic reaction studied; a part of what the Benvenuto group likes to classify these as the simple six ligand reactions. **(1)** aniline, **(5)** 2-hydroxy-napthaldehyde, to form **(6)** 1-[(E)-(phenylimino)methyl]-2-naphthol.

Computational Methods

Computational chemistry is applied in both of these projects to determine the viability of the formation of product. Also, calculating electronic structures allowed for the observation of spectroscopy data that may be compared to spectroscopy data of synthetic material. Calculations were completed using Gaussian 09 structure package.

Gaussian 09 is the latest version of the Gaussian® series of electronic structure programs. Starting from the fundamental laws of quantum mechanics, Gaussian 09 predicts the energies,

molecular structures, vibrational frequencies and molecular properties of molecules and reactions in a wide variety of chemical environments. Gaussian 09 models can be applied to both stable species and compounds which are difficult or impossible to observe experimentally (e.g., short-lived intermediates and transition structures). These calculations define wave functions for atoms and molecules and incorporated to the electronic calculations via *ab initio* calculations ("ab initio is Latin for "from the beginning", meaning starting from the fundamental time-independent Schrodinger equation and including no experimental data). It is not only with inorganic chemistry can computational chemistry provides answers. Advancements towards the development of computational chemistry are provided by the Nobel Prize winning theoretical chemist, John A. Pople, pioneering the development of *ab initio* quantum mechanics computational methods. Programs such as Gaussian would not be in existence. It is with his co-authorship that the first Gaussian program became the primary source of calculative, model chemistry.[14] Furthermore, methods of computational chemistry have been widely applied and are deemed suitable for small molecules as well as large biological systems. This has been illustrated by a second set of Nobel prize winning research of Karplus and Warshel.[15] Hartree-Fock and DFT approximations to the wave function are produced by the electronic structure calculations. Since the Schrodiner equation can't be solved exactly, approximations are needed. The Hartree Fock and density functional methods are a type of calculation set up within Gaussian in order to approximate the ground-state wave function and ground-state energy of a quantum many-electron system. Density functional methods such as B3LYP are inexpensive ways of including in the calculations electron interactions that would otherwise be neglected by Hartree Fock calculative methods.[16] Both methods build molecular orbitals from sets of base functions of atoms within the molecule. Distinct computational details for projects A and B follow.

Project A: Geometries of structures of the C_2H_2 ligand, C_2H- and complexes of cations with C_2H_2 and C_2H- were optimized using the Hartree Fock method with QZVP basis sets. Frequency calculations

determined the zero point energy, and enthalpy of optimized structures of calculations on cations, C_2H2, C_2H- complexes of cations with C_2H_2 and C_2H.

Project B: Fe^{3+} was calculated, and structures for a model ligand and an Fe^{3+} ligand complex were optimized with Hartree Fock method and 6-31G(d) basis set. Geometries of ligands and complexes with Fe^{3+} were optimized using both the Hartree Fock method and B3LYP method along with a 6-31G(d) basis set. Frequency calculations determined zero point energy, thermal correction to enthalpy, Gibbs free energy, E, H, S, the change in Gibbs free energy, and the change in enthalpy. The same calculations are presented for Z^{2+}.

Experimental Method for Project B:

The following reagents and solvents were used in order to complete the synthesis of **(3)** and **(6)** as shown in **Figure 2.** Both reactions required a one to one molar ratio of aniline to salicylaldehyde or 2-hydroxy-napthaldehyde, respectively, dissolved in approximately 15 mL of 95% ethanol. The procedure of the reaction for both of the ligand syntheses follows.

The round bottom flask for each reaction was washed out with acetone and dried in an oven for about 5 minutes. Once the round bottom flasks were completely dried, they were set aside on the cork ring stands. Then, the stir bars were gathered and submerged in acetone as well and set to dry in order to completely sterilize and remove any residue that may alter the NMR spectra. Next, the reagents were measured out and placed in the round bottom flask. The dry reagents were placed first (aniline). Then, the aqueous reagents were measured out in a tared sample vial. Both reagents, dry and aqueous, were combined and the ethanol was the last substance poured into the round bottom flask before the stir bars were placed inside the flask. The stir plate was turned on. No heat was applied to the reaction as it took place at room temperature. The stir plate and round bottom flask were left to stir for over 24 hours without any temperature changes. Once the solution had completely dissolved, it was attached to a

rotary evaporator in order to remove all organic solvent used in the reaction environment. Once the rotary evaporator could no longer extract any solvent, the resin-type substance was left to sit for about 48 hours to air dry. Once this was complete and crystal formation was evident, the sample was collected into a sample vial. Another smaller sample was taken away from the stock sample and placed in a separate vial and dissolved with about 2 mL of deuterated methylene chloride. A pipette filtration system was set up as follows: one pipette was filled with a small piece of Kimwipe in order to create a filtration system that emptied out into the capillary. Once the ligand had dissolved in the solvent, it was filtered into the capillary via the pipette filtration system and then capped and set for spectroscopic analysis. Then, proton NMR was ran and spectra were measured. The same solvent was then used to generate the solutions used for the IR spectra.

Computational results

Project A: The change in energy and enthalpy for acetylene complex formation reactions and for deprotonation reactions are calculated from the data collected. **Table 1** shows the calculated M052X/QZVP energetic of the formation of the metal-acetylene complex. This data suggests that all the complexes listed form readily, because the change in enthalpy for the formation of the complex is negative. **Table 2** shows the change in energy due to deprotonation for acetylene and metal-acetylene complexes. This data suggests that all the complexes listed deptrotonate readily, because the change in enthalpy for the reaction is positive. It can be understood that the lower the enthalpy of reaction for removal of an H^+, the greater is the relative ease of deprotonation of the complex. This data suggests that the acetylene complexes with zinc and nickel deprotonate most readily. **Figures 3-9** displayed the bond lengths and angles of the final metal-acetylene complexes optimized. The complexes shown fall into two categories that correlate to the tables provided. The complexes on the left are metal acetylene complexes before deprotonation and the complexes on the right of the page are the metal acetylene

complexes that have been deprotonated. These calculations failed to locate and optimize any complexes of C_2H_2 with metals with a charge greater than 2^+. These cations have large charge/size rations and might be expected to form stable complexes with C_2H_2.

Table 1: Calculated M052X/QZVP energies of the formation of the metal-acetylene complex.

Reaction	ΔE_0 (HF)	ΔE_0 Kcal/mol	ΔH_{298}(HF)	ΔH_{298}Kcal/mol
Cu + C2H2 -> Cu^+C2H2	-0.064	-40.11	-0.065	-40.78
Zn + C2H2 -> $Zn^{2+}C2H2$	-0.171	-107.6	-0.172	-108.2
Cd + C2H2 -> $Cd^{2+}C2H2$	-0.143	-89.55	-0.144	-90.15
Ni + C2H2 -> $Ni^{2+}C2H2$	-0.141	-88.27	-0.138	-86.67
Fe + C2H2 -> $Fe^{2+}C2H2$	-0.140	-88.12	-0.142	-88.80
Mn + C2H2 -> $Mn^{2+}C2H2$	-0.125	-78.20	-0.126	-78.81

Table 2 Table 2: Calculated M052X/QZVP energies of the deprotonation of the metal-acetylene complex.

Reaction	ΔE_0 (HF)	ΔE_0 Kcal/mol	ΔH_{298}(HF)	ΔH_{298}Kcal/mol
C2H2->C2H- + H+	0.598	375.5	0.601	376.9
CuC2H2 -> CuC2H + H+	0.348	218.7	0.351	220.1
CdC2H2 -> CdC2H + H+	0.120	75.03	-0.144	76.33
ZnC2H2 -> ZnC2H + H+	0.101	63.36	0.103	64.65
NiC2H2 -> NiC2H + H+	0.083	51.93	0.085	53.27
$Fe^{2+}C2H2$ -> $Fe^{2+}C2H$ + H+	0.126	79.16	0.121	76.05
$MN^{2+}C2H2$ -> $Mn^{2+}C2H$ + H+	0.130	81.51	0.132	82.83

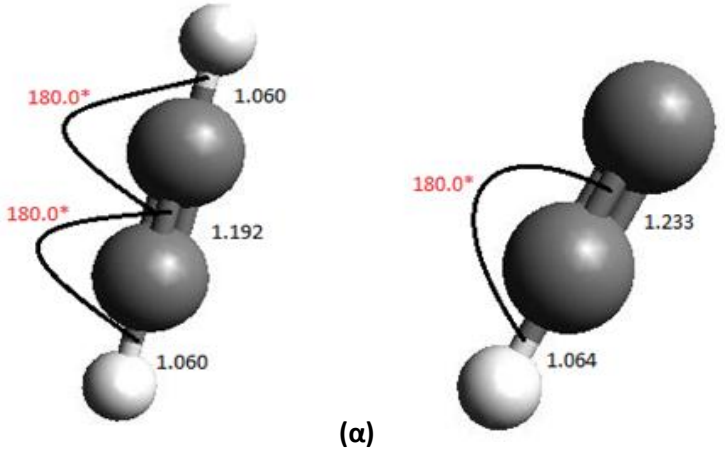

Figure3: (α) Acetylene ligand before metal atom attachment and deprotonation. **(β)** Acetylene ligand after deprotonation. Each structure remains linear; the bond lengths are of the lowest energy structure optimized during calculation. Structures were optimized with HF/QZVP calculations. All bond lengths are in angstroms and all angles are in degrees.

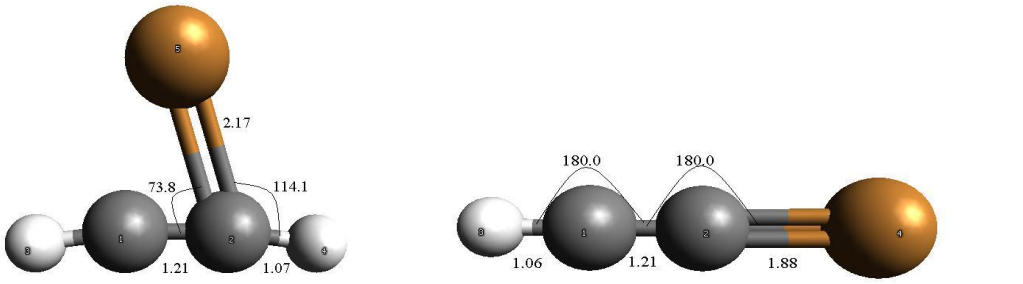

(α) **(β)**

Figure4: (α) Acetylene complex with copper (+) atom attachment before deprotonation. **(β)** Acetylene complex after deprotonation. Each structure remains linear, the bond lengths are of the lowest energy structure optimized during calculation. Structures were optimized with HF/QZVP calculations. All bond lengths are in angstroms and all angles are in degrees.

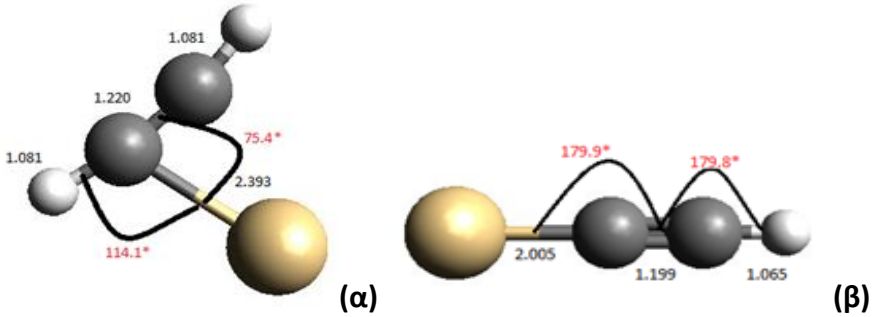

(α) **(β)**

Figure5: (α) Acetylene complex with cadmium (2+) atom attachment before deprotonation. **(β)** Acetylene complex after deprotonation. Each structure remains linear with bond angles in red text, the bond lengths are of the lowest energy structure optimized during calculation. Structures were optimized with HF/QZVP calculations. All bond lengths are in angstroms and all angles are in degrees.

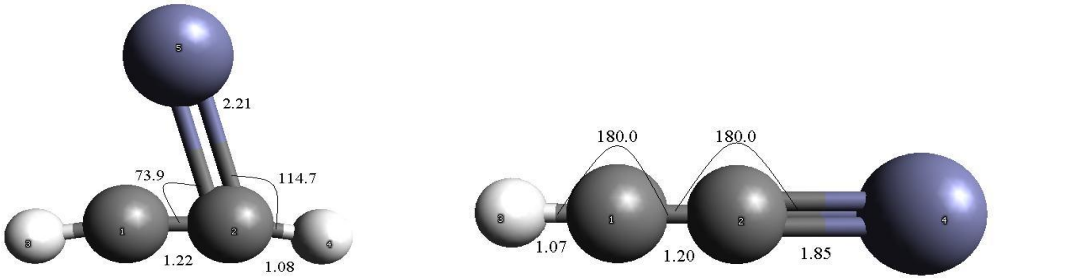

(α) **(β)**

Figure6: (α) Acetylene complex with zinc (2+) atom attachment before deprotonation. **(β)** Acetylene complex after deprotonation. Structures were optimized with HF/QZVP calculations. All bond lengths are in angstroms and all angles are in degrees.

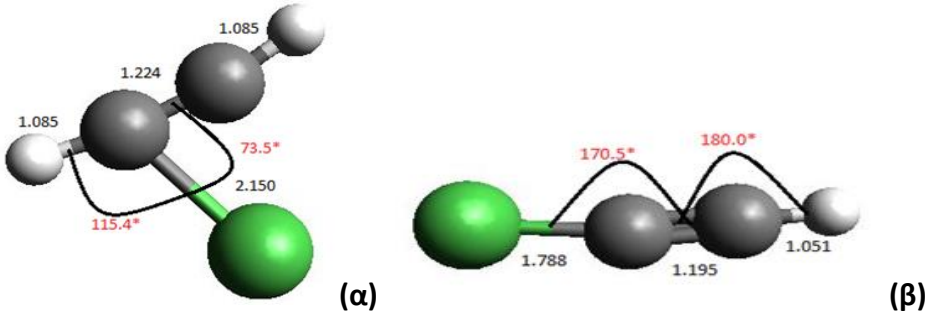

Figure 7: (α) Acetylene complex with nickel (2+) atom attachment before deprotonation. **(β)** Acetylene complex after deprotonation. Structures were optimized with HF/QZVP calculations. All bond lengths are in angstroms and all angles are in degrees.

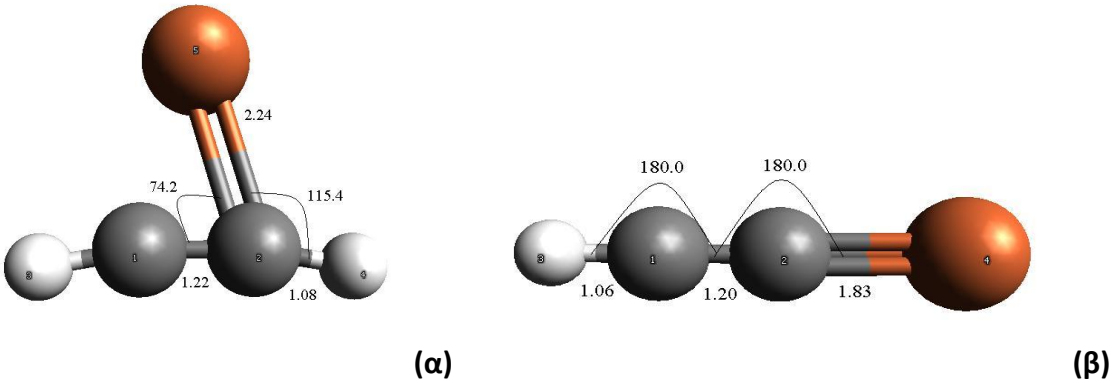

Figure 8: (α) Acetylene complex with iron (2+) atom attachment before deprotonation. **(β)** Acetylene complex after deprotonation. Structures were optimized with HF/QZVP calculations. All bond lengths are in angstroms and all angles are in degrees.

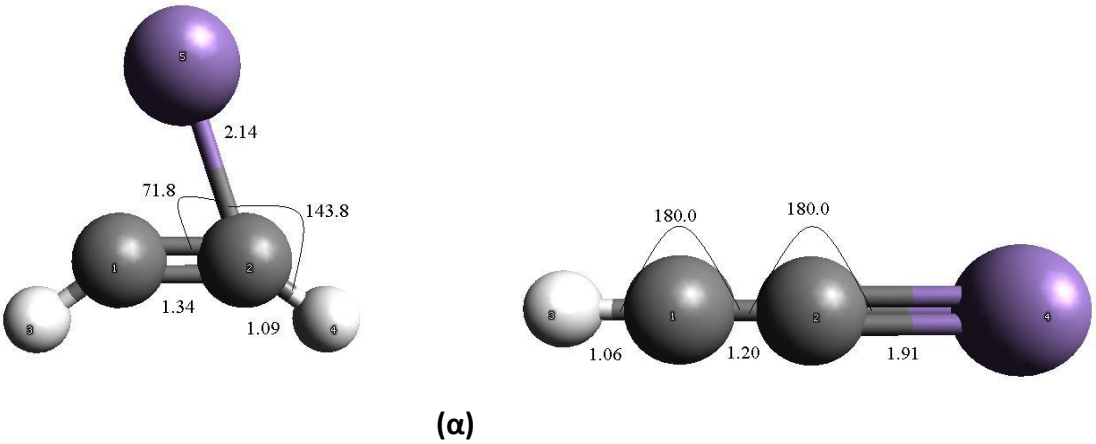

Figure 9: (α) Acetylene complex with manganese (2+) atom attachment before deprotonation. **(β)** Acetylene complex after deprotonation. Structures were optimized with HF/QZVP calculations. All bond lengths are in angstroms and all angles are in degrees.

Project B: Table 3 displays computed energies of the two metals analyzed, Fe^{3+} and Zn^{2+}**.** Four optimized structures of one ligand, L2, (**L2-1, L2-2, L2-3, L2-4**) are represented by **Figure 10,** respectively. Their relative energies of L2-2 throughout L2-4 in comparison with L2-1 are presented in **Table 4**. The two conformers with the lowest energy without a hydrogen bond to a donor atom are **L2-2 and L2-3.**These two were chosen because they were the two ligands with the lowest energy without a hydrogen bond to a donor atom. The complex structures of these ligand structures to Fe^{3+}, **Fe-C2-1** and **Fe-C2-2** are shown in **Figure 11**. This figure displays various views of the optimized complex of Fe^{3+} to the ligand. The Fe^{3+} ion, in theory, did attach to the ligand by use of the Hartree Fock computational method. In both figures the interaction with the benzene ring as Fe3+ binds to the ligand structure is observed. The red box around the sp3 carbon displays this. Complexes with Fe3+ were optimized. Energies are presented in **Table 5**. The complexes have a similar shape and orientation to the conformation of the ligand before chelation. Further calculations were completed with different model ligands shown in **figures 13-15**, correlating to the structure of the byproduct in question. The relative energies of the four added model ligands are presented in **Table 6.** Zn^{2+} was also optimized with all ligand structures. The results for the successful Z^{2+} calculations are presented in **Table 5 and 7.** All figures relating to the completed optimization of these structures with Zn^{2+} and Fe^{3+} are presented in figures **16-20**.

Table 3: Ionic atoms Fe^{3+} and Zn^{2+} data for calculations of both the Hartree Fock and B3LYP methods with the use of a 6-31G(d) basis set.

Ion	Fe^{3+}	Zn^{2+}
Hartree- Fock	-1260	-1777
Zero-Point Energy Correction	0	0
Thermal Correction to Enthalpy	0.0024	0.0024
E (Hartree)	-1260	-1776
H (Hartree)	-1260	-1776

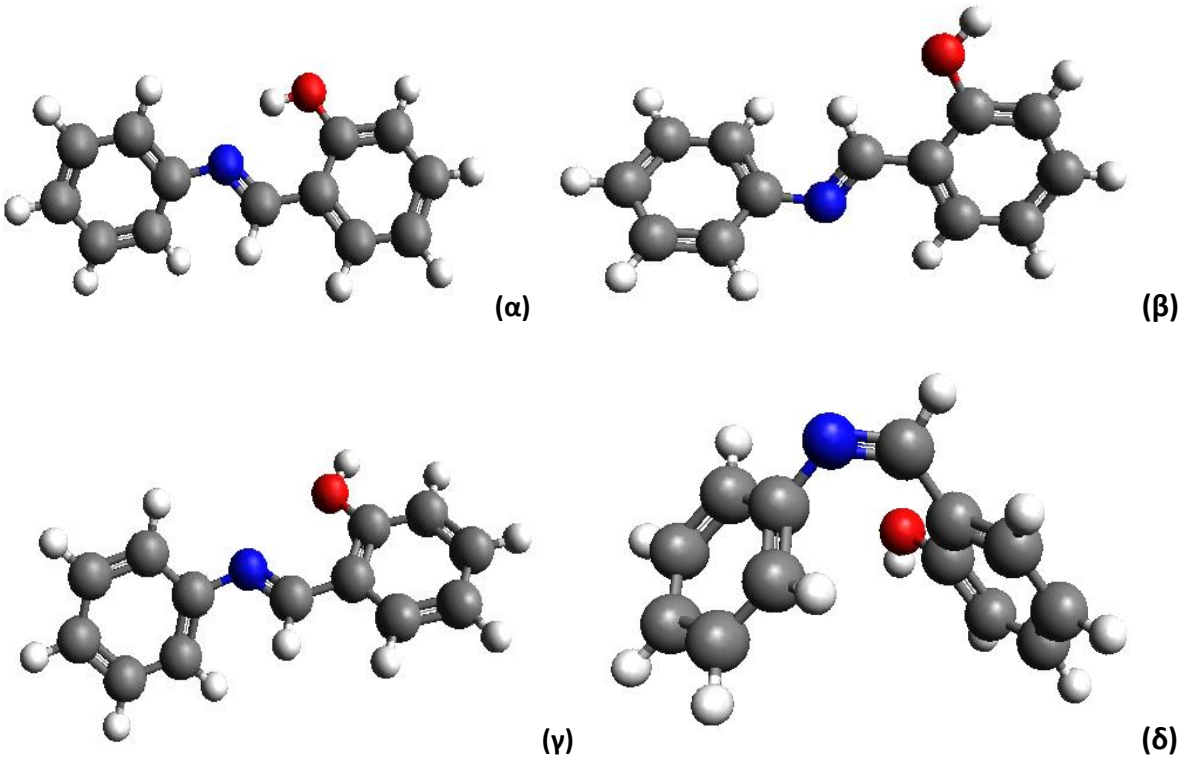

Fig 10: (α) Ligand 2-1, an isomer of L2-2, L2-3, and L2-4. This structure was optimized with both Hartree Fock and B3LYP method and a 6-31G(d) basis set. The blue atom represents the nitrogen, red represents the oxygen. **(β)** Ligand 2-2, an isomer of L2-1, L2-3, and L2-4. This structure was optimized with both Hartree Fock and B3LYP method and a 6-31G(d) basis set. The blue atom represents the nitrogen, red represents the oxygen. **(γ)** Ligand 2-3 an isomer of L2-1, L2-2 and L2-4. This structure was optimized with both Hartree Fock and B3LYP method and a 6-31G(d) basis set. The blue atom represents the nitrogen, red represents the oxygen. **(δ)** L2-4 an isomer of L2-1, L2-2, and L2-3. This structure was optimized with both Hartree Fock and B3LYP method and a 6-31G(d) basis set. The blue atom represents the nitrogen, red represents the oxygen.

Table 4: Complete data of ligand calculations for both the Hartree Fock and B3LYP methods with the use of a 6-31G(d) basis set. The relative energies in comparison to L2-1 are presented. Ligand 2 and 3 have ideal energies for complexation.

Data Points	L2-1	**L2-2**	**L2-3**	L2-4
Hartree Fock	-628.003	-627.993	-627.985	-627.978
B3LYP	-631.983	-631.967	-631.961	-631.953
Relative Energy (Hartree)	0	0.010404	0.018943	0.025485
Relative Energy (Kcal/Mol)	0	6.52879	11.88704	15.99229
With ZPE	0	5.88121	11.18110	15.15520
Relative Energy (B3LYP)	0	0.01584	0.021925	0.029828
Relative Energy (Kcal/Mol)	0	9.94561	13.75844	18.71735
With ZPE	0	9.44925	13.23699	18.05408

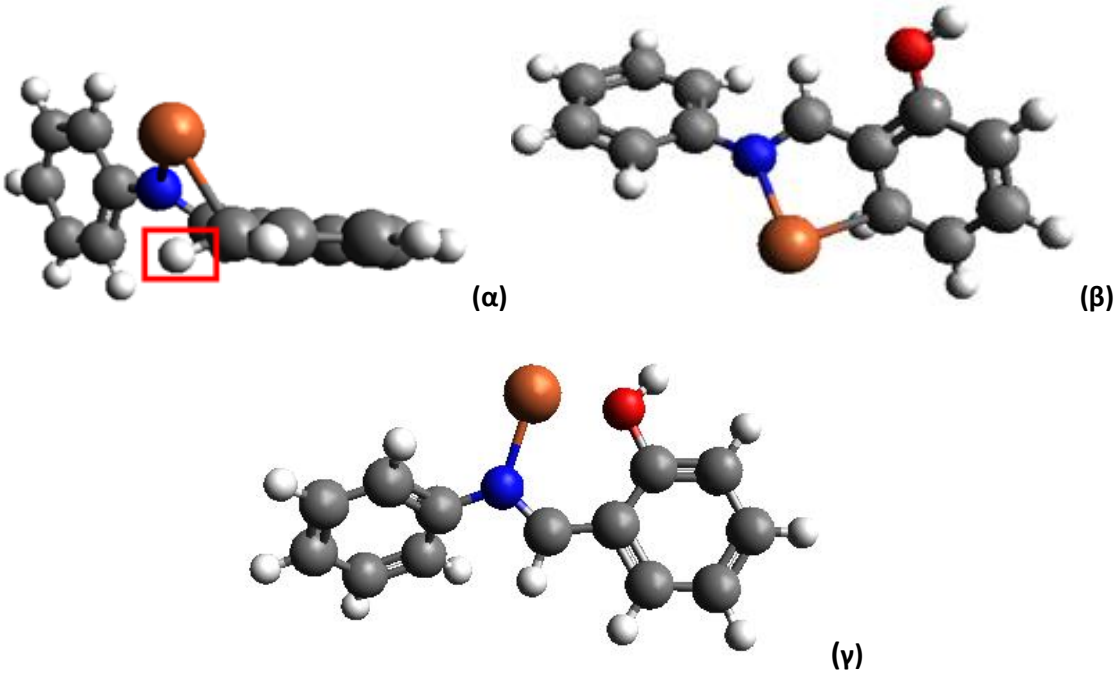

Figure 11: (α) Complex 2-1 is the L2-2 model ligand attached to Fe^{3+}. The red box signifies the sp3 hydrogen bond. The blue atom represents the nitrogen, red represents the oxygen, and the orange represents Fe^{3+}. **(β)** A second orientation of Complex 2-1 is displayed. **(γ)** Complex2-2 is the L2-3 model ligand complexed with Fe^{3+}.

Table 5: Relative energies of C2-1 and C2-2 complexes with Fe3+ and Z2+. Energies are calculated with respect to C2-1 complexes of both metals.

Complex	C2-1Fe	C2-2 Fe	C2-1Zn	C2-2Zn
Hartree Fock	-1889.25	-1889.28	-2404.91	-2404.95
Zero-Point Energy Correction	0.220612	0.22122	0.224194	0.224359
Thermal Correction to Enthalpy	0.234911	0.235403	0.237998	0.238013
Thermal Correction to Gibbs Free Energy	0.177226	0.177419	0.182881	0.18384
E (Hartree)	-1889.03	-1889.06	-2404.69	-2404.73
H (Hartree)	-1889.02	-1889.05	-2404.68	-2404.71
G (Hartree)	-1889.43	-1889.46	-2405.10	-2405.13
S (j/mol*K)	121.409	122.038	116.004	114.017
ΔH (Kcal/mol)	-513.495	-537.264	-196.303	-221.849
ΔS (Kcal/mol)	-0.006782	-0.006725	-0.007319	-0.007886
ΔG (Kcal/mol)	-511.473	-535.260	-194.122	-219.499

Table 6: Hartree Fock energies of L3 – L6.

Data point	L3 (nap1a)	L4 (benzamine)	L5 (2thienyl)	L6 (2furyl)
Hartree Fock	-780.630	-569.134	-873.716	-513.186
Zero-Point Energy Correction	0.27283	0.205698	0.18267	0.17806
Thermal Correction to Enthalpy	0.287533	0.216755	0.193515	0.188999
Thermal Correction to Gibbs Free Energy	0.230569	0.168098	0.144848	0.140215
E (Hartree)	-780.357	-568.928	-873.534	-513.008
H (Hartree)	-780.342	-568.917	-873.523	-512.997
G (Hartree)	-780.861	-569.302	-873.862	-513.326
S (j/mol*K)	119.89	102.408	102.429	102.673

Table 7: Hartree Fock energies of C4-6 complex with Zn^{2+}.

Complex	C4Zn	C5Zn	C6Zn
Hartree Fock	-2346.039	-2650.64	-2290.08
Zero-Point Energy Correction	0.206681	0.183956	0.179321
Thermal Correction to Enthalpy	0.219268	0.196324	0.191768
Thermal Correction to Gibbs Free Energy	0.166648	0.144356	0.139293
E (Hartree)	-2345.83	-2650.44	-2289.91
H (Hartree)	-2345.81	-2650.43	-2289.89
G (Hartree)	-2346.20	-2650.77	-2290.22
S (j/mol*K)	110.749	109.375	110.441
ΔH (Kcal/mol)	-183.862	-189.198	-179.494
ΔS (Kcal/mol)	-0.007180	-0.007513	-0.007317
ΔG (Kcal/mol)	-181.722	-186.959	-177.313

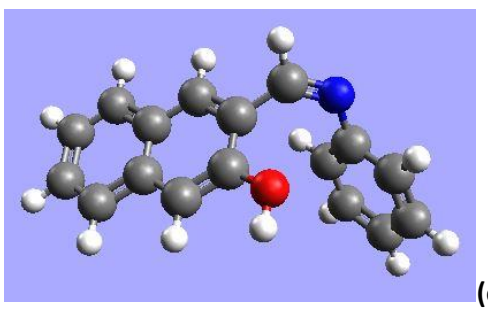
(α)
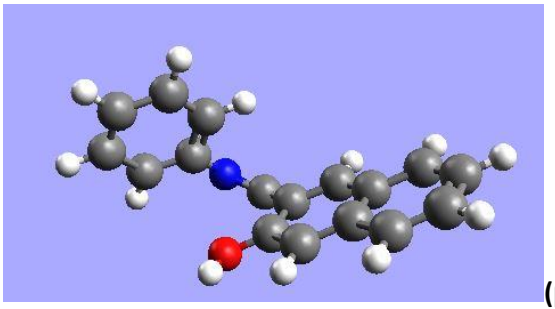
(β)

Figure 12: (α) Ligand 3, a structure known as 1-[(*E*)-(Phenylimino)methyl]-2-naphthol. The blue atom represents the nitrogen, red represents the oxygen. **(β)** A second orientation of ligand 3.

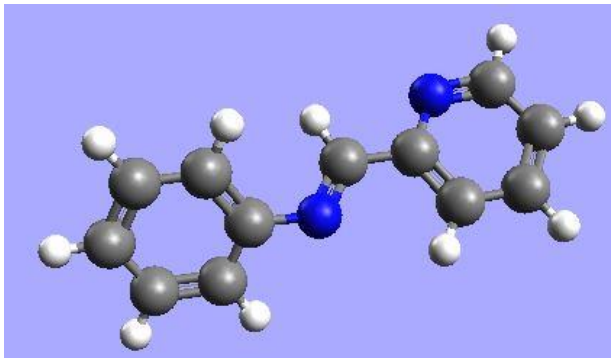

Figure 13: Ligand 4, a structure known as Benzamine. The blue atom represents the nitrogen atom.

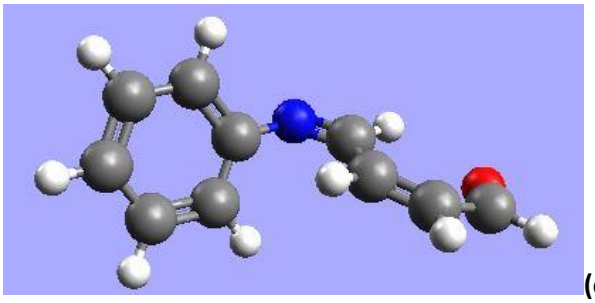
(α)
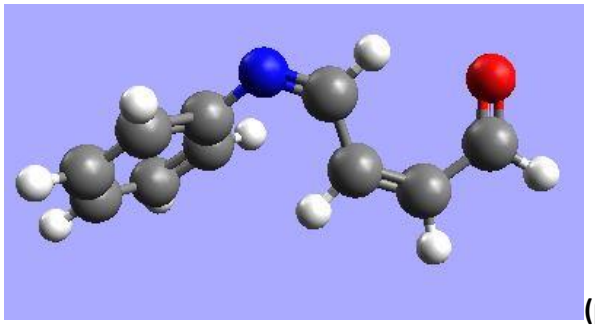
(β)

Figure 14: (α) Ligand 5, a structure known as (*E*)-1-(2-Furyl)-N-phenylmethanimine. The blue atom represents the nitrogen, red represents the oxygen. **(β)** Second orientation of ligand 5.

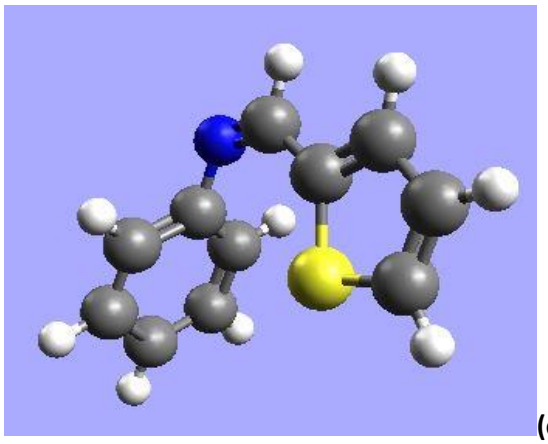
(α)
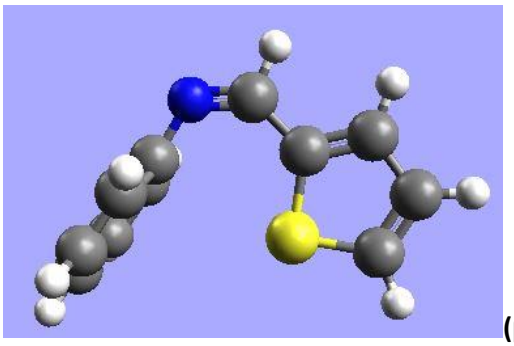
(β)

Figure 15: (α) Ligand 6, above is a structure known as 2-[(*E*)-2-(2-Thienyl)vinyl]pyridine. Two orientations **(β)** of the same structure are presented. The blue atom represents the nitrogen, red represents the oxygen, and the yellow represents sulfur.

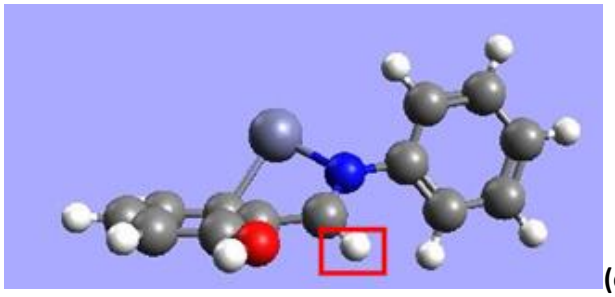
(α)
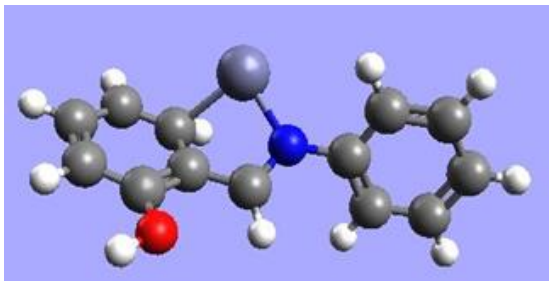
(β)

Figure 16: (α) C2-1 complex with Zn^{2+}. The red box signifies the Sp3 hydrogen bond. The blue atom represents the nitrogen, red represents the oxygen, and the purple represents Zinc. **(β)** A second orientation of C2-1 with Zn^{2+}.

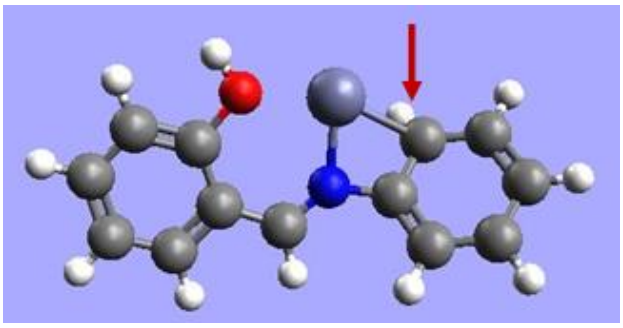

Figure 17: C2-2 complex with Zn^{2+}. The red arrow signifies the hydrogen with a sp3 bond, out of symmetry with the rest of the hydrogen atoms in plane with the ring on the right side of the figure. The blue atom represents the nitrogen, red represents the oxygen, and the purple represents Zn^{2+}.

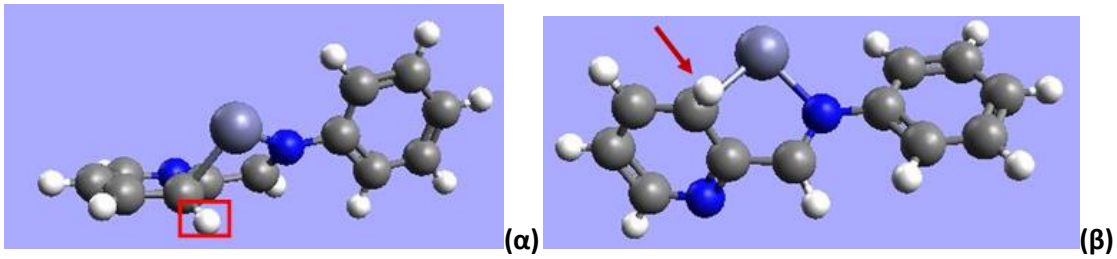

(α) **(β)**

Figure 18: (α). L4 complex with Zn^{2+}. The structure now labeled as C4, the red box signifies the Sp3 hydrogen bond. The blue atom represents the nitrogen, red represents the oxygen, and the purple represents Zinc. **(β)** A second orientation of C4 with $Zinc^{2+}$.

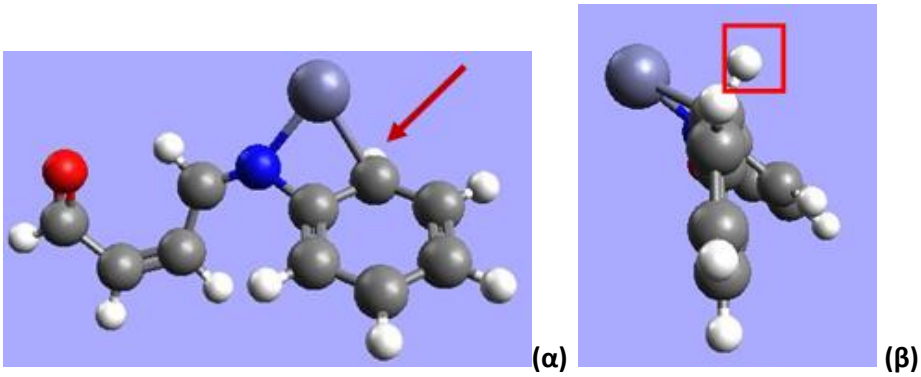

(α) **(β)**

Figure 19: (α). L5 complex with Zn^{2+}. The structure now labeled as C5, the red box signifies the Sp3 hydrogen bond out of symmetry with the rest of the hydrogen atoms in plane with the ring structure it is bonded with. The blue atom represents the nitrogen, red represents the oxygen, and the purple represents Zinc. **(β)** A second orientation of C5 with $Zinc^{2+}$

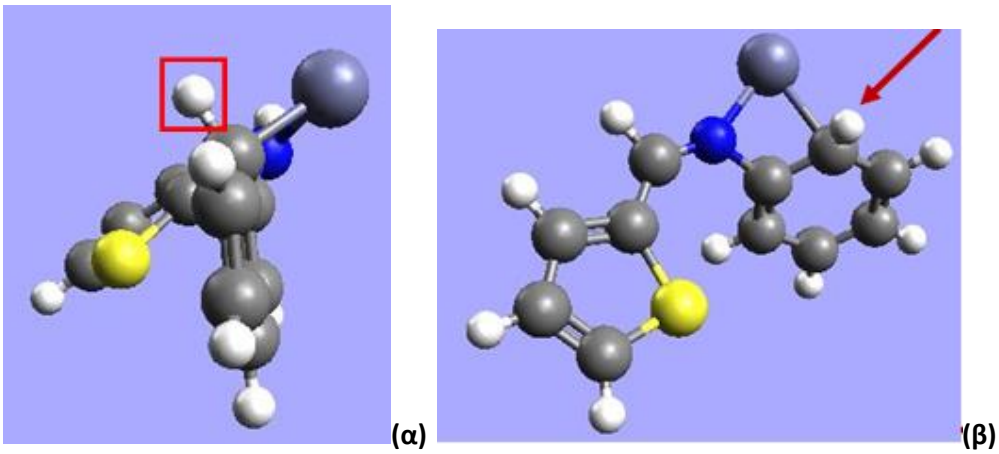

(α) **(β)**

Figure 20: (α) L6 complex with Zn^{2+}. The structure now labeled as C6, the red box signifies the Sp3 hydrogen bond out of symmetry with the rest of the hydrogen atoms in plane with the ring structure it is bonded with. The blue atom represents the nitrogen, red represents the oxygen, the purple represents Zinc, and the yellow represents a sulfur atom. **(β)** A second orientation of C6 with $Zinc^{2+}$

Experimental Results of Project B

The reactions of **scheme 1-2** were analyzed using $^{+}$HNMR and FTIR spectroscopy. These ligand models have been synthesized in order to determine whether or not a larger ligand (4, 4'-diaminodiphenylmethane) will chelate with a metal sample. Peak assignments from the H^{+}NMR (**Figure 21, Table 8-9)** describe that the experimental ligand model appropriately suits the ligand model analyzed with computations (**Figure 22-23**).

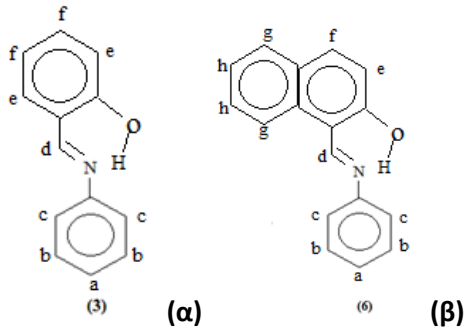

Figure 21: (α) H^{+} NMR assignment and structural representation for FT-IR for **(3)** from **Scheme 1. (β)** H^{+} NMR assignment and structural representation for FT-IR for **(6)** from **Scheme 2.**

Table 8: $^{+}$HNMR for **(3)** the proton nuclear magnetic resonance spectrometry data regarding the final structure. These were assigned based on ppm, resonance of the structure and the induction effect.

δ (ppm)	Multiplicity	Integral	Atom assignment
δ7.5-7.4	m	4	e&f
δ 7.35	d	1	d
δ7.3	m	5	c,b,a,

Table 9: $^{+}$HNMR for **(6)** The proton nuclear magnetic resonance spectrometry data regarding the final structure. These were assigned based on ppm, resonance of the structure and the induction effect.

δ (ppm)	Multiplicity	Integral	Atom assignment
δ8.1	D	1	a
δ7.45	M	4	b&c
δ7.3	S	2	g&h
δ7.1	S	1	d
δ 7.0	M	2	e&f

Table 10: FTIR for **(3)**, **(6):** The functional groups present throughout structures **(3)** and **(6)** present in **Figures 1-2** Based on IR data.

Wavenumber	Bond assignment	Wavenumber	Bond assignment
3075 cm^{-1}	C-H aromatic	3058 cm^{-1}	C-H aromatic
2884 cm^{-1}	C-H aliphatic	2973 cm^{-1}	C-H aliphatic
1615 cm^{-1}	Imine group (C-N=)	1621 cm^{-1}	Imine group (C-N=)
800-400 cm^{-1}	Benzene ring stretches	800-400 cm^{-1}	Benzene ring stretches

Figure 22: **FT-IR spectra for (3).** The red-boxed wavelengths are the most significant peaks which can be later compared with electronic vibration patterns of similar structures that have been calculated electronically.

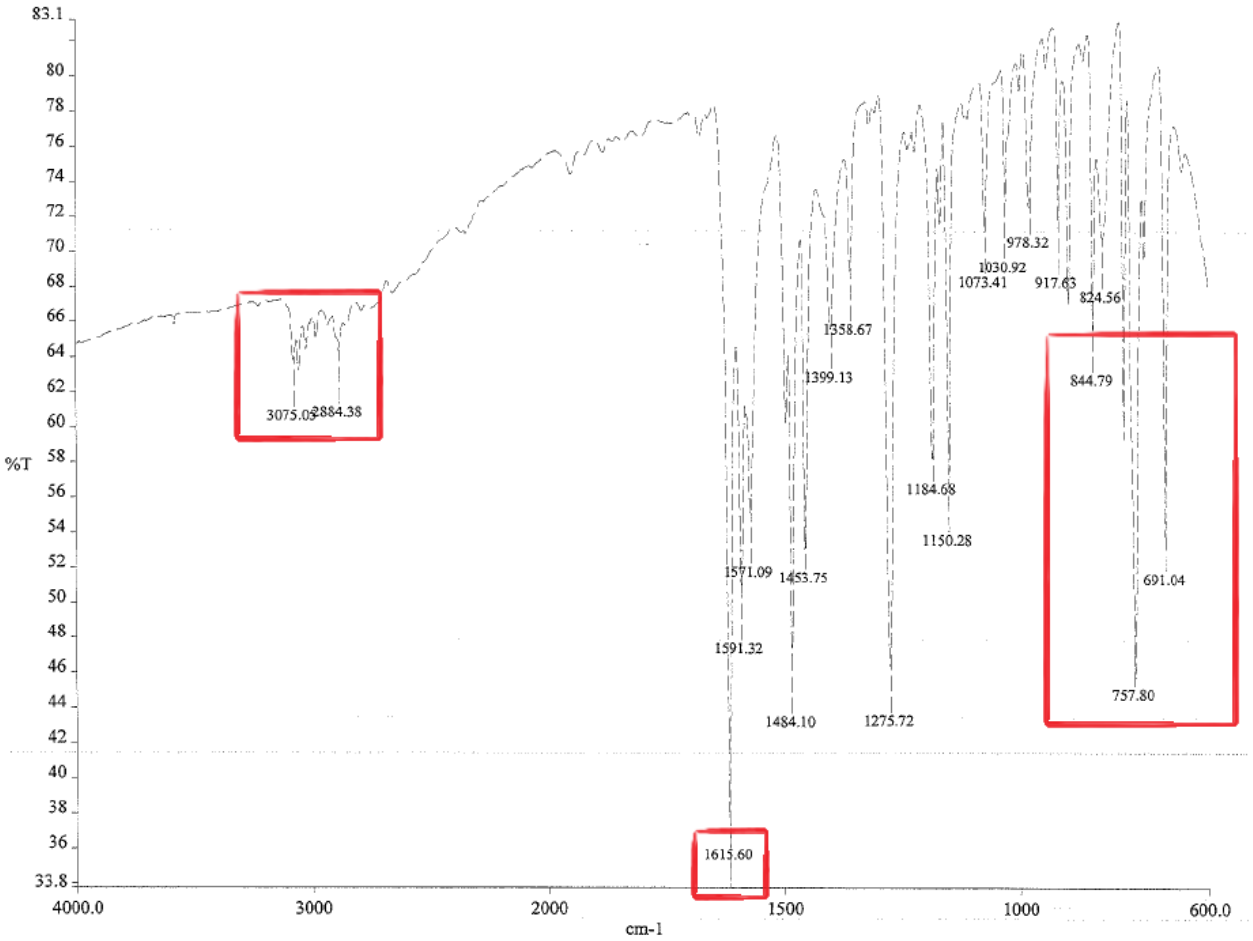

Figure 23: **FT-IR spectra for (6).** The red-boxed wavelengths are the most significant peaks which can be later compared with electronic vibration patterns of similar structures that have been calculated electronically.

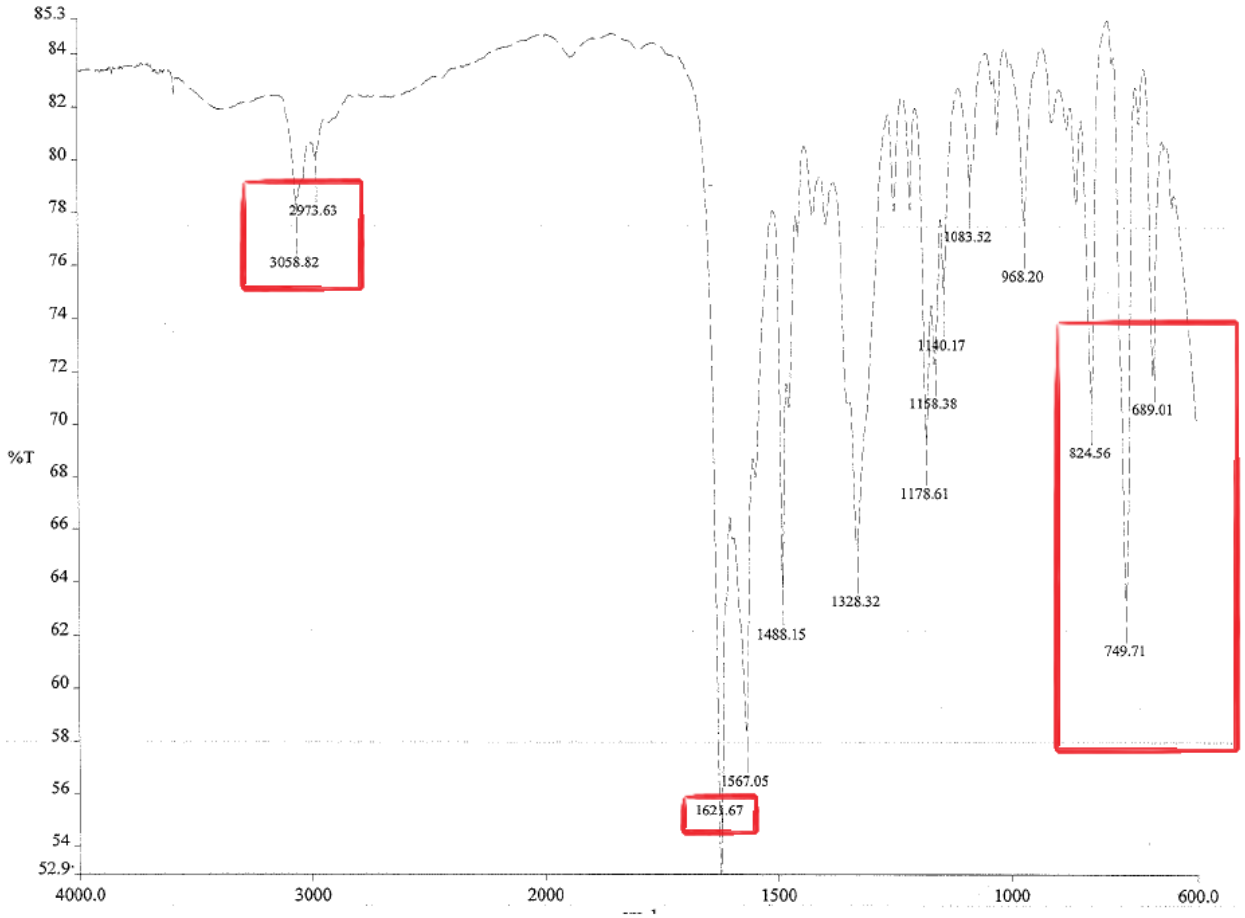

Conclusions

Both experiments yielded results that provide a great deal of feedback regarding metal co-catalysts for the Sonogashira reaction as well as chelation properties of different ligand structures. Regarding project A, it was determined that the use of zinc would enhance and cheapen the Sonogashira reaction. The use of copper is traditional, in that it has been used for decades in order to provide the best reaction environment possible. However, zinc provides a nearly identical reaction environment, with similar deprotonation energy as copper, but a less expensive material. Further experimentation will continue with different metals including nickel. Regarding project B, the ligands calculated chelate best

with iron and zinc. Although chelation was a success, synthesis has not yielded the appropriate result. Eventually, the synthesized ligands will be used to complex with period four transition metals, particularly Iron (III) and eventually lanthanides. In later experimentation, the ligands synthesized will be complexed with Iron(III) perchlorate. There are two paths followed for complexation viewed in the following schemes: **Scheme 3 and 4** is a reaction between the ligand and the triperchlorate without alteration to the ligand at hand. **Scheme 5 and 6** display the second reaction which requires the use of a carbon palladium catalyst in order to remove hydrogen from the nitrogen site on the ligand. Thus, a charge is created and a single bond is left through the nitrogen chain between the phenol groups. The change in the structure may allow for a more readily bonding ligand.

Another goal is to develop calculations employing a solvent model, in theory, to observe whether or not the energies and other components of the structure are drastically altered when water is incorporated. A model for water would be used considering the application is considered for water purification. The theory behind the application design is motivated by a product design marketed by Proctor and Gamble.[17] Designing a product that precipitates and causes coagulation of a wide range of pollutants, clean drinking water is now a realistic possibility for even the most underdeveloped nations. The idea now is to utilize the specific byproduct which the aforementioned structures are all modeled after in this same design that Proctor and Gamble have marketed. The concept is surrounded by the idea of using a material (the byproduct) without having to develop a completely new material for purification.

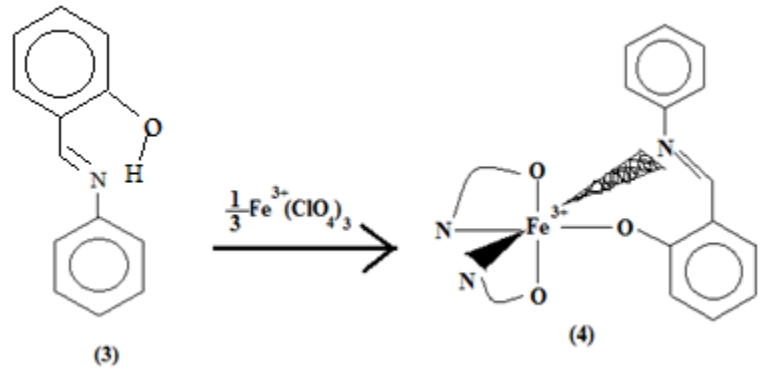

(3) (4)

Scheme 3: This is the final step of the first reaction. The complex is formed with Iron (III). **(3)** salicylideneaniline reacts with Iron (III) triperchlorate to form **(4)** IL1

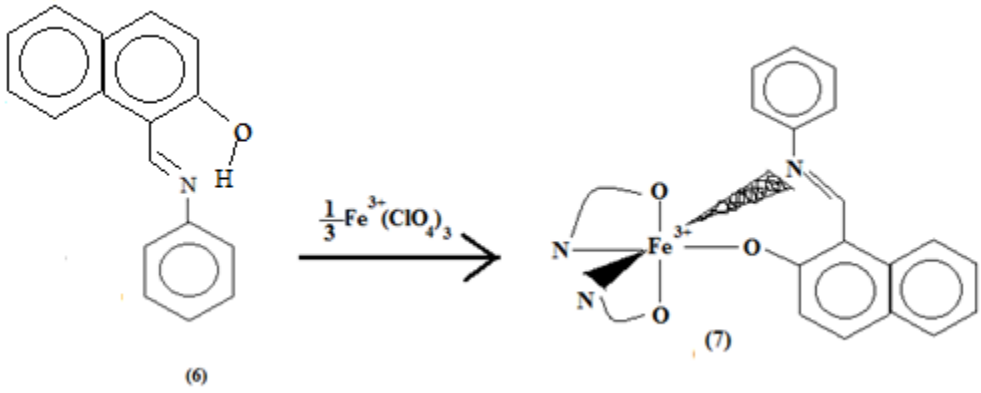

(6) (7)

Scheme 4: This is the final step of the second reaction. The complex is formed with Iron (III). **(6)** reacts with Iron (III) triperchlorate to form **(7)** IL2

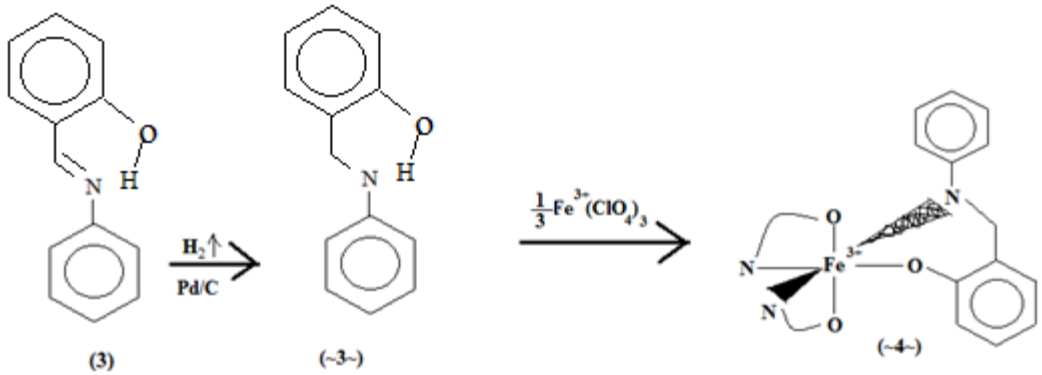

(3) (~3~) (~4~)

Scheme 5: This is the second path take, testing the final step of the first reaction. The complex is formed with Iron (III). **(3)** reacts with a palladium carbon catalyst creating a charged ligand **(~3~)** and then reacts with Iron (III) triperchlorate to form **(~4~)** IL1b

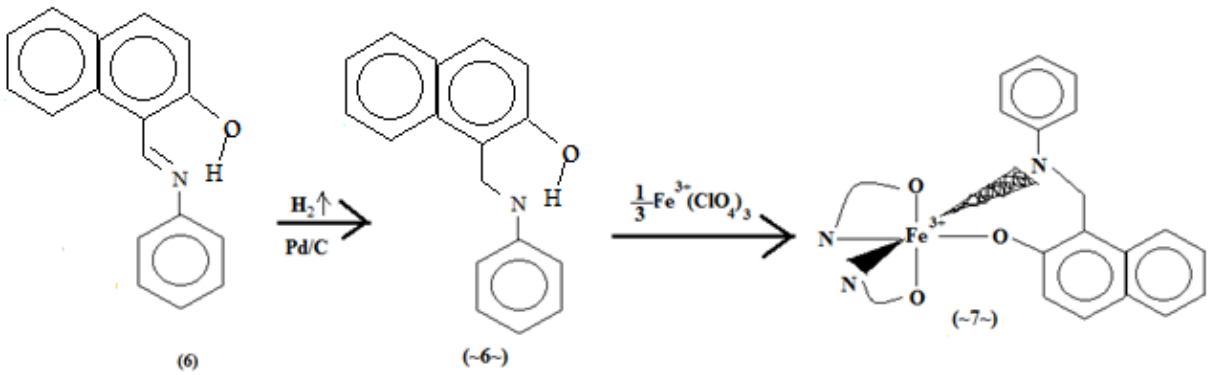

Scheme 6: This is the second path take, testing the final step of the first reaction. The complex is formed with Iron (III). **(6)** reacts with a palladium carbon catalyst creating a charged ligand **(~6~)** and reacts with Iron (III) triperchlorate to form **(~7~)** IL2b

Acknowledgments

I would like to thank the University of Detroit Mercy Department of Chemistry and Biochemistry for use of their facilities, laboratory equipment, materials, and reagents. I would also like to thank the Pittsburgh Supercomputing Center for the use of their supercomputers. Most importantly, I would like to thank my committee members: Mark A. Benvenuto, Professor of Chemistry, Matthew J. Mio, Associate Professor of Chemistry, and Shulamith S. Schlick, Professor of Chemistry.

References

1 Sonagashira, K. Development of Pd–zed cross-coupling of terminal acetylenes with sp2-carbon halides, *J. Organomet. Chem*. **2002,** *65,3* 46-49.

2 Thakur, K.G.; Jaseer, E.A.; Naidu, A.B.; Sekar, G. An efficient copper(I) complex catalyzed Sonogashira type cross-coupling of aryl halides with terminal alkynes. *Terahedron. Lett*. **2009,** *50,* 2865– 2869 .

3 Doucet, H.; Hierso, J-C.; Palladium-Based Catalytic Systems for the Synthesis of Conjugated Enynes by Sonogashira Reactions and Related Alkynylations, *Angew. Chem. Int. Ed*. **2007**, *46*, 834 – 871.

4 Chinchilla, R. ; Najera, C. The Sonogashira Reaction: A Booming Methodology in Synthetic Organic Chemistry *Chem. Rev.* **2007,** 107, 874-922.

5 Chinchilla, R.; Najera, C. Recent Advances in Sonogashira Reaction *Chem. Rev.* **2011**. *111,* 5084-5121.

6 Thakur, K.G.; Jaseer, E.A.; Naidu, A.B.; Sekar, G. *Tetrahedron Lett*. **2009,** *50,* 2865–2869 .

7 Johnson C.*; Miller M.; *J. Org. Chem.*, **1997**, *62,* pp 1582–1583

8 Liang B.; Dia M.; Chen J.; Yang Z.; *J. Org. Chem.*, **2005**, *7,0* pp 391–393

9 McCarroll A.; Bradshaw T.; Westwell A.; Matthews C.; Stevens M.; *J. Med. Chem.*, **2007**, *50* 1707–1710

10 Gising J.; Nilssons M.; Odell L.; Yahiaoui S.; Lindh M.; Iyer H.; Snhall A.; Srinivasal B.; Larhdet M.; Mowbraws S.; Karlen A.; *J. Med. Chem.*, **2012**, *55*, pp 2894–2898

11 Negishi, E; Anastasia, L. *Chem. Rev.* **2003**, *103*, 1979-2018

12 Konja A.; Stevens J.; Continuation on the Study of the Deprotonation of Transition Metal-Acetylene Complexes and Other Fe3+ Ligand-Complex Formation with Electronic Structure Calculations. *Manuscript.* 2012.

13 Chinchilla, R.; Najera, C. Recent Advances in Sonogashira Reaction *Chem. Rev.* **2011**.

14"John Pople's Career and Legacy." *John Pople's Career and Legacy*. N.p., n.d. Web. 25 Apr. 2014.

15“The Nobel Prize in Chemistry 2013". *Nobelprize.org.* Nobel Media AB 2013. Web. 25 Apr 2014. <http://www.nobelprize.org/nobel_prizes/chemistry/laureates/2013/>

16 Hehre, Warren J. *A Guide to Molecular Mechanics and Quantum Chemical Calculations*. Irvine, CA: Wavefunction, 2003. Print.

17 "PUR Packet." *PUR Packet*. N.d., Web. 24 Mar. 2014. <http://www.pg.com/pur_packet.shtml>.

18 Carril, M.; Correa, A.; Bolm, C. Iron Catalyzed Sonagashira Reactions, *Angew. Chem. Int. Ed*.

2008, *47*, 4862 –4865.

19 Plenio, H. Catalysts for the Sonogashira Coupling—The Crownless Again Shall Be King, *Angew. Chem. Int. Ed.* **2008**, *47*, 6954 –6956.

20 Volla, C.M.; Vogel, P. Iron/copper catalyzed C-C cross coupling of aryl iodides with terminal alkynes, *Tetrahedron Lett.* **2008,** *49,* 5961-5964.

21 Gaussian 09, Revision **A.1**, M. J. Frisch, G. W. Trucks, H. B. Schlegel, G. E. Scuseria, M. A. Robb, J. R. Cheeseman, G. Scalmani, V. Barone, B. Mennucci, G. A. Petersson, H. Nakatsuji, M. Caricato, X. Li, H. P. Hratchian, A. F. Izmaylov, J. Bloino, G. Zheng, J. L. Sonnenberg, M. Hada, M. Ehara, K. Toyota, R. Fukuda, J. Hasegawa, M. Ishida, T. Nakajima, Y. Honda, O. Kitao, H. Nakai, T. Vreven, J. A. Montgomery, Jr., J. E. Peralta, F. Ogliaro, M. Bearpark, J. J. Heyd, E. Brothers, K. N. Kudin, V. N. Staroverov, R. Kobayashi, J. Normand, K. Raghavachari, A. Rendell, J. C. Burant, S. S. Iyengar, J. Tomasi, M. Cossi, N. Rega, J. M. Millam, M. Klene, J. E. Knox, J. B. Cross, V. Bakken, C. Adamo, J. Jaramillo, R. Gomperts, R. E. Stratmann, O. Yazyev, A. J. Austin, R. Cammi, C. Pomelli, J. W. Ochterski, R. L. Martin, K. Morokuma, V. G. Zakrzewski, G. A. Voth, P. Salvador, J. J. Dannenberg, S. Dapprich, A. D. Daniels, Ö. Farkas, J. B. Foresman, J. V. Ortiz, J. Cioslowski, and D. J. Fox, Gaussian, Inc., Wallingford CT, **2009**.